University of Baghdad
College of Engineering
JE
JOURNAL OF ENGINEERING

Journal of Engineering

journal homepage: www.jcoeng.edu.iq

Volume 32 Number 11 November 2026

Core-Scale Modeling and Numerical Simulation of Alanine-Based Deep Eutectic Solvent Flooding for Enhanced Oil Recovery: An Experimental and Simulation Case Study of the Mishrif Reservoir, West Qurna-2 Oil Field, Southern Iraq

Elaf Q. Attieh [1, 2, *], **Hussein Q. Hussein** [1], **Anfal K. Shebli** [3]

[1] Department of Chemical Engineering, College of Engineering, University of Baghdad, Baghdad, Iraq
[2] Missan Oil Training Institute, Ministry of Oil, Missan, Iraq.
[3] Petroleum Research and Development Center, Ministry of Oil, Baghdad, Iraq.

ABSTRACT

This study investigates the performance of an amino acid deep eutectic solvent (ADES) made of alanine and choline chloride as a green displacement solvent to the Mishrif carbonate reservoir, based on a laboratory-calibrated numerical model. The goals were to measure the interfacial tension (IFT), and wettability response of the ADES/crude oil/carbonate system, to replicate the core flooding experiment in the CMG-STARS software. The IFT and contact angle show a decrease from 4.22 mN/m and 103° to 1.00 mN/m and 8.4°, respectively, as the concentration of ADES was raised from 0 to 250 ppm. A one-dimensional Cartesian model (50 x 1 x 1) maintaining the bulk volume, pore volume, cross-sectional area, and length of the cylindrical plug was developed in CMG-STARS; wettability alteration was modeled by linear interpolating between the oil-wet and water-wet relative permeability; and chemical retention was modeled by a CMG adsorption isotherm. Brine flooding recovered 58% of OOIP and reduced oil saturation from 0.690 to 0.290; tertiary ADES injection at 150 ppm raised recovery to 73%, an incremental 15 percentage points of OOIP and a 36% reduction of residual oil saturation to 0.186. The history-matched model reproduced the measured recovery factor within 5 percentage points and the differential pressure within 6.5 percentage points. The main contribution of this work is the integration of experimentally measured IFT and contact angle into relative permeability interpolation for ADES flooding in an Iraqi carbonate system and the demonstration that wettability alteration, rather than IFT reduction, controls the incremental recovery in this system.

Keywords: Amino Acid DESs, Carbonate reservoir, CMG-STARS, Core flooding, Enhanced oil recovery.

*Corresponding author
Peer review under the responsibility of University of Baghdad.
https://doi.org/10.31026/j.eng.2026.11.08
This is an open access article under the CC BY 4 license (http://creativecommons.org/licenses/by/4.0/).
Article received: 13/07/2026
Article revised: 15/09/2026
Article accepted: 15/09/2026
Article published: 01/11/2026

1. INTRODUCTION

As global energy demand continues to rise and conventional reservoirs become increasingly mature, the development of advanced enhanced oil recovery (EOR) technologies has become increasingly important. The recovery of oil by primary and secondary recovery methods typically only recovers about 30-40% of the original oil, depending on the reservoir properties and oil fluid characteristics **(Hasan, 2022; AL-Dujaili et al., 2026).** The rest of the oil remains in the pore structure due to low displacement efficiency, capillary forces, unfavorable wettability, and interfacial tension **(Boon, 1984; Biyouki et al., 2025)**. Therefore, chemical enhanced oil recovery (CEOR) technologies, such as surfactant, polymer, and alkaline technologies, have become an important means to enhance the microscopic oil displacement efficiency and mobilize residual oil **(Lwisa, 2021).**

The injection of chemical additives such as surfactants, polymers, alkalis, ionic liquids, and others has been widely studied for the purpose of lowering the interfacial tension, altering the rock wettability, controlling the mobility of fluids in the rock, and improving oil displacement, among the various CEOR methods **(Salih et al., 2016)**. However, most traditional chemical products have problems with environmental pollution, toxicity, poor biodegradability, poor thermal stability, and low activity in harsh reservoir conditions such as high salinity and high temperature. These restrictions have stimulated research into more environmentally friendly and sustainable alternatives that can achieve high recovery efficiency while keeping the environmental impact to a minimum **(Atilhan and Aparicio, 2021).**

Recently, deep eutectic solvents (DESs) have emerged as a new family of green solvents that can be applied in chemical enhanced oil recovery. Typically, these solvents are made up of an H-bond donor (usually a urea, ethylene glycol, glycerol, or an organic acid or amino acid) and an H-bond acceptor (usually a choline chloride). The resulting eutectic mixture has a melting point significantly lower than the melting point of the elemental components, and it is a stable liquid that has a different physicochemical structure from the components **(Velez and Acevedo, 2022).**

Experimental investigations and numerical studies have indicated that DESs can achieve increased oil recoveries by several mechanisms: reduction in the interfacial tension, changing the wettability from oil-wet to water-wet, viscosity reduction of heavy crude oil, and improvement in the mobility ratio. Further, desirable properties of DESs include high thermal stability, very low vapor pressure, low toxicity, biodegradability, and relatively low production costs, which are desirable properties for use as alternatives to the conventional EOR chemicals **(Hamdi et al., 2020; Kumar et al., 2025; Raut et al., 2023).**

Recently, special focus has been given to natural deep eutectic solvents such as amino acid-based deep eutectic solvents prepared from natural components (choline chloride and amino acids). These solvents exhibit high hydrogen-bonding potential, good environmental behavior, and outstanding physicochemical stability. Amino acid-based DESs have also shown that they can significantly change the wettability of carbonate rocks by lowering the contact angle between the injected aqueous phase and rock surfaces and make the two interact more. Because of their environmentally friendly properties and good thermal stability, they are good candidates for sustainable chemical EOR **(Husain and Abu-Jdayil, 2025).**

Laboratory core flooding experiments provide direct evidence of chemical flooding performance, but they are limited to certain rock-fluid type operating conditions and can sometimes require time and resources. Therefore, numerical reservoir simulation has

become an essential tool for assessing chemical flooding performance under a variety of reservoir conditions and also has reduced the cost and experimental time in the laboratory. The simulation of the numerical model allows researchers to explore the effect of chemical concentration, injection rate, slug size, reservoir temperature, salinity, adsorption behavior, and rock-fluid interaction prior to pilot-scale or field-scale applications **(Goudarzi et al., 2016; Jalil and Hussein, 2018).**

The most common commercial reservoir simulator for chemical enhanced oil recovery modelling is considered to be the simulator developed by CMG (Computer Modelling Group) called CMG-STARS (Computer Modelling Group–Steam, Thermal, and Advanced Processes Reservoir Simulator). The simulator can simulate complex multiphase flow phenomena, adsorption, wettability alteration, reduction of interfacial tension, alteration of relative permeability, transport and reaction of chemicals. It has been successfully used to simulate several types of core flooding experiments performed in the laboratory, including polymer, surfactant, ionic liquids, nanoparticles, and other chemical flooding processes. CMG-STARS can be used to match data obtained from the laboratory with the field data to accurately calibrate reservoir properties and predict the performance of various chemical injection strategies prior to implementation in the field **(Elaghoury et al., 2022; Kumar and Mandal, 2017).**

Despite the growing interest in deep eutectic solvents (DESs) for potentially sustainable use as EOR chemicals, the literature on EOR using DESs is largely limited to conventional choline chloride-based systems and other eutectic formulations and has focused on their experimental results, interface characteristics, and oil-displacement mechanisms. Molecular dynamics simulations of the interaction of aqueous choline-based DESs with oil in calcite-assisted EOR have been shown to be important in considering the role of interfacial tension reduction, hydrogen bonding, and wettability alteration in DES-assisted EOR **(Kumar et al., 2025).** Additionally although there are few examples of numerical workflows to reproduce laboratory core-flooding experiments and optimize the parameters of the chemical slug, these numerical workflows are demonstrated only for surfactant and conventional CEOR systems **(Kumar and Mandal, 2020).** Hence, the development and validation of a CMG-STARS workflow to simulate laboratory core flooding experiments with choline chloride–amino acid deep eutectic solvents is a relatively limited research path. The workflow can offer a quantitative framework to correlate the experimentally measured physicochemical properties and the interfacial properties with the transport and displacement behavior of alanine-based deep eutectic solvent (ADES) at the core scale and facilitate systematic optimization of chemical concentration, salinity, and injection condition.

The specific objective of this study is to develop a history-matched core-scale numerical model by using the CMG-STARS simulator that relates the experimentally determined core-scale physicochemical, interfacial tension reduction, and wettability alteration properties with the ADES ability to displace oil in carbonate cores. The carbonate core flooding experiment was built up in CMG-STARS, and the resulting model was validated by history matching relative permeability curves.

2. MATHEMATICAL MODEL

2.1 Governing Equation

The CMG-STARS reservoir simulator was used to implement the numerical simulation of the ADES flooding experiment. The governing equations describing the multiphase flow and chemical transport in porous media are solved using a finite-difference formulation by the

CMG-STARS simulator **(Aziz and Settari, 2002).** The simulator solves the mass conservation equations for all chemical components simultaneously with Darcy's flow equation. It includes adsorption, diffusion/dispersion, chemical reactions, phase behavior, and source/sink terms from injection and production wells. These coupled equations comprehensively represent chemical EOR processes in carbonate **(Chen et al., 2006; Imankulov et al., 2021).**

The mass conservation equation for component i in a system of n components distributed among the flowing phases α (α = water, oil) is that the rate of accumulation is equal to the net influx by convection and dispersion of the component plus the net rate of injection or production of the component. This is expressed by Eq. (1) **(Aziz and Settari, 2002; Goudarzi et al., 2016):**

$$\frac{\partial}{\partial t}[\, V_f \sum_\alpha (\rho_\alpha S_\alpha C_{i,\alpha}) + V_r A d_i] = \sum_\alpha \nabla.(T_\alpha \rho_\alpha C_{i,\alpha} \Delta\varphi_\alpha) + \sum_\alpha \nabla.(\emptyset D_{i,\alpha} \rho_\alpha \nabla C_{i,\alpha}) + \sum_\alpha \rho_\alpha q_\alpha C_{i,\alpha} \quad (1)$$

Where:

V_f is the fluid volume of the grid block,

V_r is the rock volume

$\rho_\alpha, S_\alpha, C_{i,\alpha}$ are the density saturation mass fraction of the component i in phase α

Ad_i is the adsorbed concentration of component i

T_α is the phase transmissibility

$\Delta\varphi_\alpha$ is the phase potential difference

$D_{i,\alpha}$ is the dispersion/diffusion coefficient

$\emptyset$ is the porosity

q_α represents the well rate. The formulation allows the simulator to properly model the transport of the injected ADES during the chemical flooding process (CMG STARS Technical Manual)**(Delshad et al., 1996; Lake et al., 2014)**. In Eq. (1), all terms involving energy and a gas phase are omitted because the core-flooding experiment simulated here was carried out under isothermal conditions with dead oil and no free gas phase. No geochemical reactions were included in the model, so the reaction source/sink term is likewise omitted. Darcy velocity (u_α) is used to describe the fluid flow in porous media, in which the fluid velocity relates to absolute and relative permeability, fluid viscosity, pressure drop, and gravitational effects as written in Eq. (2) **(Cazarez-Candia et al., 2012):**

$$u_\alpha = -\frac{k\, k_{r\alpha}}{\mu\alpha}(\nabla P_\alpha - \rho_\alpha g \nabla z) \quad (2)$$

Where:

k,$k_{r\alpha}$ are the absolute and relative permeability, respectively.

μ_α is the fluid viscosity

P is the pressure.

g is the gravitational acceleration.

By substituting Eq. (2) into Eq. (1), for a horizontal one-dimensional flow, in which the gravitational term vanishes, Eq. (1) is rearranged to yield Eq. (3).

$$\frac{\partial}{\partial t}(\emptyset \rho_\alpha S_\alpha) = \frac{\delta}{\delta x}\left(\frac{k\, k_{r\alpha} \rho_\alpha}{\mu\alpha}\frac{\delta P_\alpha}{\delta x}\right) + q_\alpha \quad (3)$$

The one-dimensional representation is used since the radial flow in the core plug is very small compared to the axial flow **(Kumar and Mandal, 2020).**

The transport of the ADES as a component of the aqueous phase is governed by Eq. (1). For clarity, its transport is written explicitly in Eq. (4), which accounts for convection, hydrodynamic dispersion, and retention on the rock surface:

$$\frac{\partial(\varphi C)}{\partial t} + \nabla.(uC) = \nabla.(D\nabla C) - R_{ads} \quad (4)$$

Where:
C is the ADESs concentration in the aqueous phase.
D dispersion coefficient
R_{ads} is the rate of loss by adsorption.
The retention on the rock surface term is related to C by Eq. (5):

$$R_{ads} = \rho_r(1-\varphi)\frac{\partial C_{ads}}{\partial t} \quad (5)$$

Where:
ρ_r is the rock grain density
C_{ads} is the adsorbed concentration that described by the linear isotherm, Eq. (6):

$$C_{ads} = K_d C \quad (6)$$

Where K_d is the adsorption coefficient. The amount of active chemical available for altering wettability and lowering interfacial tension is influenced by adsorption.
CMG-STARS uses a few empirical correlations to describe the interactions between the fluids and rocks, in addition to the basic conservation equations. One of these, Corey's correlation, is used to create relative permeability curves that describe multiphase flow behavior in porous media as a function of the normalized fluid saturation. This correlation is especially helpful when there are no experimental relative permeability curves available or laboratory studies of these curves are impractical. **(Corey, 1977)** expressed the Corey relative permeability correlations by using Eqs. (7) and (8):

$$k_{rw} = k_{rwior}\left(\frac{S_w - S_{wcrit}}{1 - S_{wcrit} - S_{oirw}}\right)^{N_w} \quad (7)$$

$$k_{ro} = k_{rocw}\left(\frac{S_o - S_{wor}}{1 - S_{wcon} - S_{orw}}\right)^{N_{ow}} \quad (8)$$

Where:
k_{rw} is the water phase relative permeability.
k_{ro} is the oil phase relative permeability
S_w is the water saturation
S_{wcrit} is critical water saturation.
S_{wcon} is the connate water saturation.
S_{oirw} is the irreducible oil saturation.
S_{orw} is the residual oil saturation.
k_{rocw} is k_{ro} at connate water saturation.
k_{rwiro} is k_{rw} at irreducible oil saturation.
N_w is the exponent for calculating k_{rw} from k_{rwiro}
N_{ow} is the exponent for calculating k_{row} from k_{rocw}

Eqs (7) and (8) describe a single wettability and interfacial-tension state. The two relative permeability datasets, Set A (high-IFT oil-wet condition during waterflooding) and Set B (low-IFT water-wet condition created by ADES), are then used to interpolate between these two states, with the value of the interpolation parameter as -5 for both wetting and non-wetting phases. The interpolation is related to the capillary number, the ratio between the viscous forces and the capillary forces, which is expressed by Eq. (9):

$$N_C = \frac{u\,\mu_w}{\gamma cos\theta} \tag{9}$$

Where:
γ is the interfacial tension between the oil/ aqueous phase
θ is the contact angle with the carbonate surface
It should be noted that any decrease in γ and θ achieved by the ADES will increase N_C and also cause a shift towards the water-wetting phase in the relative permeability; the measured values of γ and θ are reported in **Table 1**.
The dimensionless interpolation parameters are computed as a function of the capillary number by using Eqs. (10) and (11) **(Kumar and Mandal, 2020):**

$$ratw = \frac{log_{10}(N_c) - DTRAPWA}{DTRAPWB - DTRAPWA} \tag{10}$$

$$ratn = \frac{log_{10}(N_c) - DTRAPNA}{DTRAPNB - DTRAPNA} \tag{11}$$

DTRAPWA (-5) and DTRAPWB (-2) are interpolation parameters denoting low capillary number for high interfacial tension values and high capillary number for low interfacial tension values, respectively, for the wetting phase. DTRAPNA (-5) and DTRAPNB (-2) are analogous interpolation terms for the non-wetting phase. Consequently, one relative permeability dataset for high interfacial tension (IFT) values during water flooding and another for low IFT values during surfactant flooding are employed to interpolate the relative permeability for intermediate IFT values, which is subsequently utilized in simulation.
The interpolation weights follow from Eqs. (12) and (13), and the interpolated relative permeabilities from Eqs. (14) and (15):

$$wtr = ratw^{WRCV} \tag{12}$$

$$oil = ratn^{OCRV} \tag{13}$$

$$k_{rw} = k_{rwA}(1 - wtr) + k_{rwB}.wtr \tag{14}$$

$$k_{ro} = k_{roA}(1 - oil) + k_{roB}.oil \tag{15}$$

Where:
$ratw\ and\ ratn$ are the dimensionless interpolation parameters which range between 0 and 1, are used to control the interpolation between different relative permeability datasets.
WRCV and OCRV are curvature interpolation parameters, which specify the shape of the interpolated relative permeability curves, and are assumed to be 1 under default conditions. WRCV and OCRV values of (1) and (1) were used so that the interpolation is linear. $k_{r\alpha}$ from Eqs. (14) and (15) return to Eq. (2).

To accurately represent the dynamic behavior of fluid flow at the core scale, the dependence of fluid density and viscosity on pressure difference was incorporated into the numerical model, rather than treating them as independent parameters. Under isothermal conditions ($\rho_i(T)$, and $\mu_i(T)$ are constant), the liquid density for each component (oil, ADES solution) is simulated as a linear exponential function of pressure based on the components compressibility in Eq. (16) **(Liu et al., 2021)**:

$$\rho_i(P) = \rho_{ref} \exp[C_{P,i}(P - P_{ref})] \quad (16)$$

Where:
$\rho_i(P)$ is the fluid density at the current reservoir pressure
ρ_{ref} is the stock tank density at reference pressure (P_{ref} =101.3x10^3 Pa)
$C_{P,i}$ is the isothermal fluid compressibility coefficient (4.35x10^{-7} kPa^{-1} for ADES solutions, 1.16x10^{-6} kPa^{-1} for oil)
P, P_{ref} are the current and refrence reservoir pressures ($P_{ref} = 101.3$ kPa $= 14.7$ psi)
When $C_{P,i} \ll 1$ Eq. (16) is rearranged to Eq. (17):

$$\rho_i(P) = \rho_{ref}[1 + C_{P,i}(P - P_{ref})] \quad (17)$$

The core flooding experiment and simulation was performed at an isothermal temperature of 25 °C. The crude oil viscosity was experimentally measured as 15.21 cP at 22.3 °C, while its density was 0.904 g/cm^3. A direct experimental relation between pressure and viscosity was not available, as no experimental measurement of the viscosity of oil as a function of pressure was available. Thus, the measured viscosity was used as a reference viscosity at the specified reference conditions, and the pressure dependence was modeled with a first-order pressure-dependence model. The viscosity was calculated by Eq. (18) **(Little and Kennedy, 1968):**

$$\mu_i(P) = \mu_{ref}[1 + B_{P,i}(P - P_{ref})] \quad (18)$$

Where:
$\mu_i(P)$ is the fluid viscosity at the current reservoir pressure
μ_{ref} is the fluid viscosity at reference pressure (P_{ref})
$B_{P,i}$ is the pressure dependence coefficient of viscosity ($B_{P,i} \ll 1$)
P, P_{ref} are the current and refrence reservoir pressures.
Because the simulations were performed at a constant temperature, no temperature-dependent variation of viscosity was introduced.

3. MATERIALS AND METHODS

3.1 Materials

3.1.1 Alanine-Based Deep Eutectic Solvent

In this study, an amino acid-based deep eutectic solvent (ADES) was used as a chemical flooding agent, which was synthesized by using alanine and choline chloride. The summary of the ADES physiochemical properties used in the numerical simulation is given in **Table 1**. It should be noted that the reported density and viscosity correspond to the density and viscosity of the ADES solution after dissolution in brine

Table 1. The ADES Physiochemical Properties

Property	Value
HBD	Alanine
HBA	Choline chloride
Molar ratio	1 : 1
Density (kg/m³)	1050
Viscosity (cP)	1.02
Studied Concentrations (ppm)	0, 50, 100, 150, 200, 250

3.1.2 Crude Oil

The crude oil was obtained from the West Qurna-2 oil field in the south of Iraq, Basra. Before the experimental operation, the crude oil was purified, centrifuged at 5000 rpm, and then filtered to remove any suspended impurities and had an API gravity of 25.01°, a density of 0.904 g/cm^3, and a viscosity of 15.21 cP at 22.3 °C. This pretreatment was done to maximize the stability of the sample and reduce the risk of asphaltene precipitation during the storage of the sample and during core flooding experiments.

3.1.3 Carbonate Core Sample

Carbonate core plugs were obtained from the Mishrif formation of the West Qurna-2 oil field. The West Qurna Oilfield is situated approximately 14 km away from the city of Qurna at the northern edge of Basrah Governorate. This oilfield represents the extension of the giant North Rumaila Oilfield in southern Iraq. The core plugs in this study were obtained from the Mishrif Formation (Wasia Group, Middle Cretaceous) **(Al-Dujaili et al., 2023).** The location of the study area is shown on **Fig. 1.**

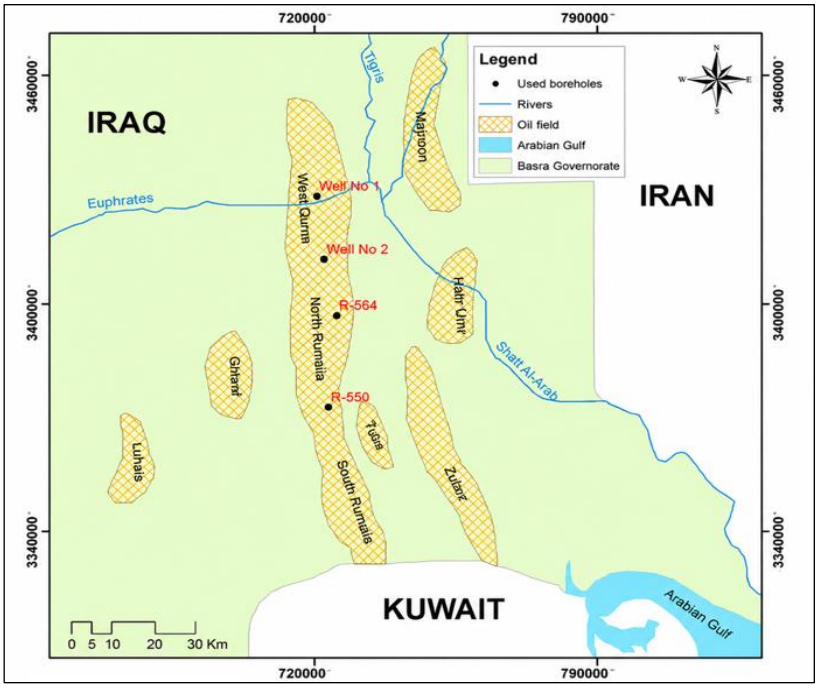

Figure 1. The Geographical Location of the Study Area in Southern Iraq **(Al-Dujaili et al., 2023)**

The cores were first cleaned by toluene and methanol using a Soxhlet extractor and dried at 60 °C until a constant weight was achieved to remove any excess fluids, salts, and other contaminants. Each core plug's porosity and absolute permeability was calculated according to the standard core analysis methods. The porosity was measured by formation water vacuum saturation, and the permeability was determined by formation water injection using the core flooding unit. Physical characteristics of core samples are given in **Table 2**. One of the raw oil-saturated carbonate core samples was sliced and polished carefully to achieve the contact angle measurements.

Table 2. Physical Characteristics of Core Samples

Property	Value
Lithology	Carbonate (Limestone)
Diameter	3.8 cm
Length	5.5 cm
Porosity	21%
Absolute permeability	67 mD
Confining pressure	500 psi
Core pressure	14.7 psi
Rock Compressibility	$4.5x\ 10^{-6}\ pa^{-1}$
Depth	2250m
Temperature	25°C
Initial water saturation (S_{wi})	0.31
Bulk Volume (BV)	$62.34cm^3$
Pore Volume (PV)	$13.1cm^3$
Injection Flow Rate	$10\ cm^3/hr$

3.1.4 Brine Formulation

The ion compositions of the brine used in the laboratory core flooding experiments and numerical simulation are listed in **Table 3**.

Table 3. The Brines Ion Compositions

Ion (ppm)	Brine 1
Na^+	3498
Cl^-	3976.66
Mg^{+2}	348.37
Ca^{+2}	1334.01
SO_4^{-2}	4678
TDS (ppm)	13835.04

3.2 Contact Angle and Interfacial Tension Measurements

Contact angle and interfacial tension (IFT) were measured by the One Attention Theta lite optical tensiometer (Biolin Scientific, Sweden), as shown in **Fig. 2**. The pendant-drop method was used to determine the IFT between the crude oil and ADES/brine solutions, whereas the contact angle was measured using the sessile-drop method on the carbonate core surface fragment. For contact-angle measurements, the carbonate core fragment was immersed in the studied solution of ADES, a droplet of distilled water was placed on the dried polished carbonate surface, and the droplet profile was captured and analyzed optically to determine

the equilibrium contact angle **(Buyukozer Ozkan et al., 2024; Abdullah et al., 2026)**. The same optical tensiometer was used to characterize both interfacial and wetting properties of the investigated systems. The measurement was against ADES concentration, and the results are listed in **Table 4**. The CMC of ADES was determined experimentally from the concentration-dependent in IFT measurements. The IFT values were plotted as a function of ADES concentration, and the CMC was identified from the intersection point of the two fitted regions before and after the change in the slope of the IFT–concentration curve. This analysis resulted in a CMC of approximately 200 ppm.

Figure 2. Contact Angle and Interfacial Tension Measurements Unit

Table 4. The Measured Values of Contact Angle and Interfacial Tension for ADES/Oil/Carbonate Surface Systems

ADES Concentration (ppm)	Interfacial Tension, γ mNm^{-1}	Contact Angle θ °
0	4.22	103
50	3.93	67.3
100	3.59	42.7
150	1.8	37.2
200 (CMC)	1.1	20.5
250	1	8.4

3.3 Core Flooding Procedure

To assess the performance of the ADES for enhanced oil recovery, core flooding experiments were performed on carbonate core plugs in the Postgraduate Laboratory, Department of Petroleum Engineering, University of Baghdad **(Alameedy et al., 2023).** A Mishrif limestone core plug was prepared and subjected to core flooding at 25 °C, 500 psi confining pressure, and at a constant pore volume injection rate of 10 cm^3/h: the injected brine (TDS = 13,835 ppm) was pumped to 2 PV, and then the ADES solution was pumped to 4 PV.

The core samples were first saturated with formation water to calculate the absolute permeability of the core sample by the injection of brine solution at a steady flow rate, and then crude oil was injected into the cores to create an initial oil saturation. **Fig. 3** represents the experimental setup of core flooding. The cumulative oil recovery factor obtained from the experiments was then used for history matching of the CMG-STARS numerical simulation model prior to the sensitivity analysis.

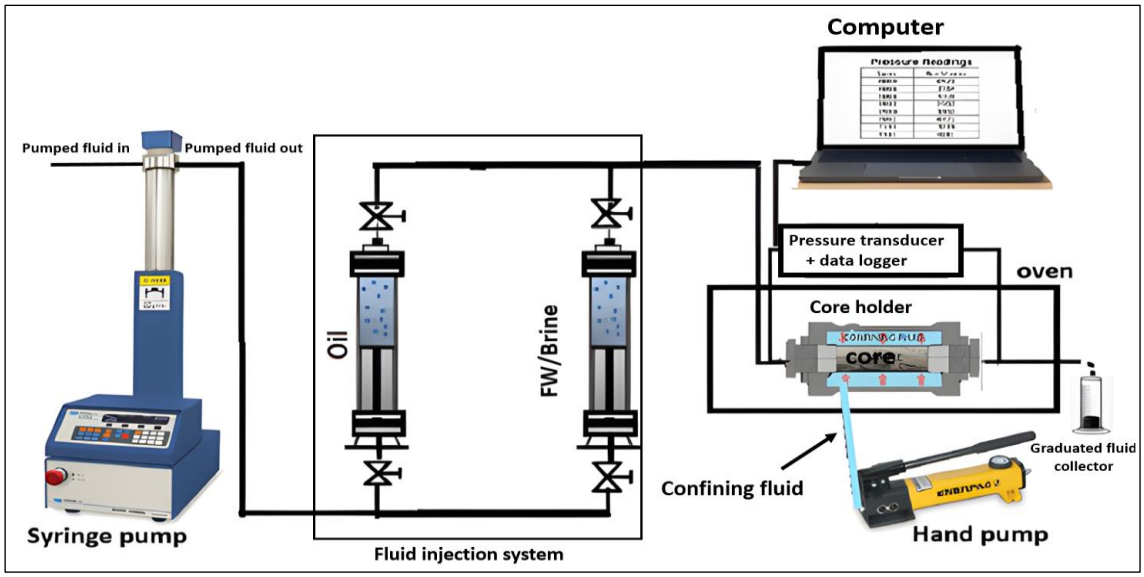

Figure 3. Experimental Setup of Core Flooding.

3.4 Simulation Methodology

The cylindrical core sample of carbonate was simulated in the simulator by employing a 1D Cartesian grid to mimic the linear flow of the fluids from the injector to the producer as it was in the lab core flooding setup. The flow direction (I-direction) was divided into 50 grid blocks, and, as it was assumed that there is no flow in the transverse (J-direction) and vertical (K-direction), only one grid block was assigned in these directions. The simulation model was built in a similar manner to the lab experiments. The volume of the rectangular grid is equivalent to the bulk volume of the cylindrical core sample. The equivalent dimensions are determined by Eq. (19):

$$V_{Cyl} = \frac{\pi D^2}{4} L \tag{19}$$

The equivalent area is calculated by Eq. (20):

$$A_{eq} = \frac{V_{Cyl}}{L} = \frac{\pi D^2}{4} \tag{20}$$

The equivalent width is calculated by Eq. (21):

$$W_{eq} = \sqrt{A_{eq}} \tag{21}$$

This gives approximately $Weq = 3.367\ cm$

The computational grid was first generated based on the core dimensions, and the rock properties, such as porosity, absolute permeability, pore volume, and rock compressibility, were determined based on measurements. The fluid properties, such as density, viscosity, relative permeability, and capillary pressure functions, were then introduced with the help of the experimental data. Initial conditions were set by injecting formation brine to saturation and then crude oil injection to get the initial water saturation (S_{wi}). Then water flooding was simulated for secondary recovery and followed by tertiary flooding using the best ADES (150 ppm <CMC dissolved in brine with 13835.04 ppm) solutions injected at the same rate as used in the experiment to residual oil saturation. The concentration of 150

ppm was selected as the optimum concentration based on its position below the CMC, the statistical analysis, and its satisfactory performance in core-flooding experiments. It should be noted that the simulation procedure was carried out as outlined in the CMG instruction manual for core-flooding experiments and chemical-flooding simulations using the CMG-STARS software.

The impact of ADES on oil recovery was modeled by adding experimentally determined wettability alteration and reduced IFT to the model. The wettability alteration was simulated by modifying the relative permeability curves to represent the transition from oil-wet to more water-wet, and the IFT reduction was implemented by using experimental data. Additionally, chemical retention due to adsorption on the carbonate rock surface was modeled by including adsorption isotherms available in CMG-STARS to represent the adsorption of ADES on the carbonate rock surface during transport through the porous medium. The cylindrical core sample, 3D model, and the grid dimension calculations are shown in **Fig. 4**.

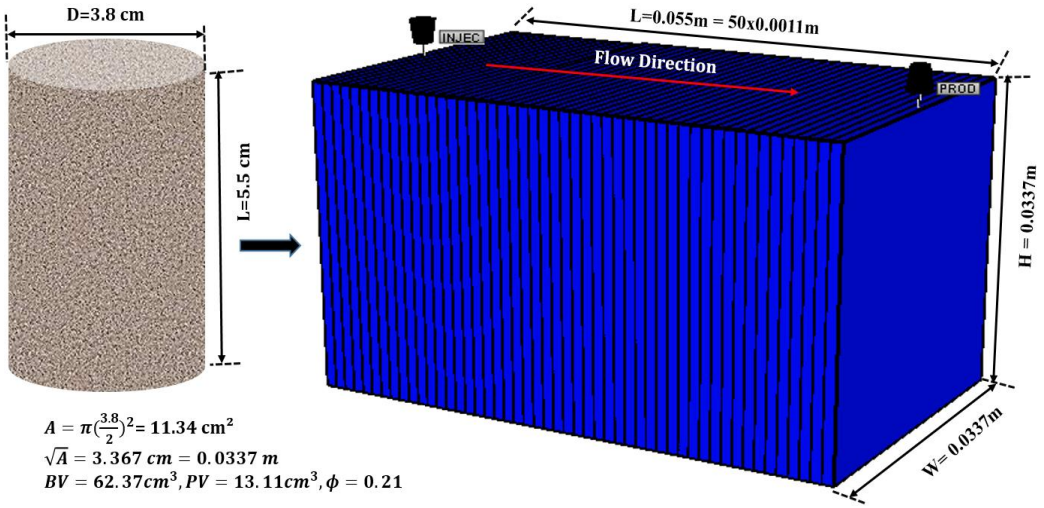

Figure 4. Equivalent Cartesian Grid Representation of the Cylindrical Core Plug

4. RESULTS AND DISCUSSION

4.1 History Matching Between the Core Model and the Lab Core

The relative permeability curves were chosen as input parameters to adjust since they were one of the most uncertain parameters in reservoir simulation, and they are highly sensitive to the pore-scale flow behavior. Several factors affect the relative permeability, such as wettability, pore structure heterogeneity, capillary pressure, and interactions between fluids and rocks **(Goudarzi et al., 2016; Zhao et al., 2024; Akbar et al., 2026)**, rendering it difficult to accurately derive from laboratory measurements alone.

In general, the final history-matched model was found to be in good agreement with the experimental data for relative permeability curves and for oil production rate as shown in **Figs. 5 and 6**, which suggests that the adjusted relative permeability curves used to simulate the multiphase flow behavior in the porous medium under the flooding conditions investigated were adequate.

Fig. 6 shows the comparison between the experimental and simulated oil recovery factor and pressure drop against the injected pore volumes of brine (until 2 PV) and ADES (injected from 2 PV to 4 PV). Water flooding recovered 58% of OOIP by 2 PV, reducing oil saturation

from 0.690 to 0.290. The ADES injection raised recovery to 73% by 4 PV, an incremental 15 % of OOIP and a 36% reduction in residual oil saturation, to 0.186. The pressure drop is divided into three stages. The early peak at 59 psi and 0.5 PV corresponds to the lowest total mobility at the highest water saturation (S_{wi}) and relates to water breakthrough, after which the mobility decreases to 52 psi at 2 PV. The renewed increase from 2 PV is exactly in the time of the ADES injection. The increase is near the viscosity of the brine, so it is not due to the viscosity of the injectant, and the increase is the same as that of an oil bank and of a change from the high-IFT, oil-wet set to the low-IFT, water-wet set, where the water relative permeability is lower for a given water saturation.

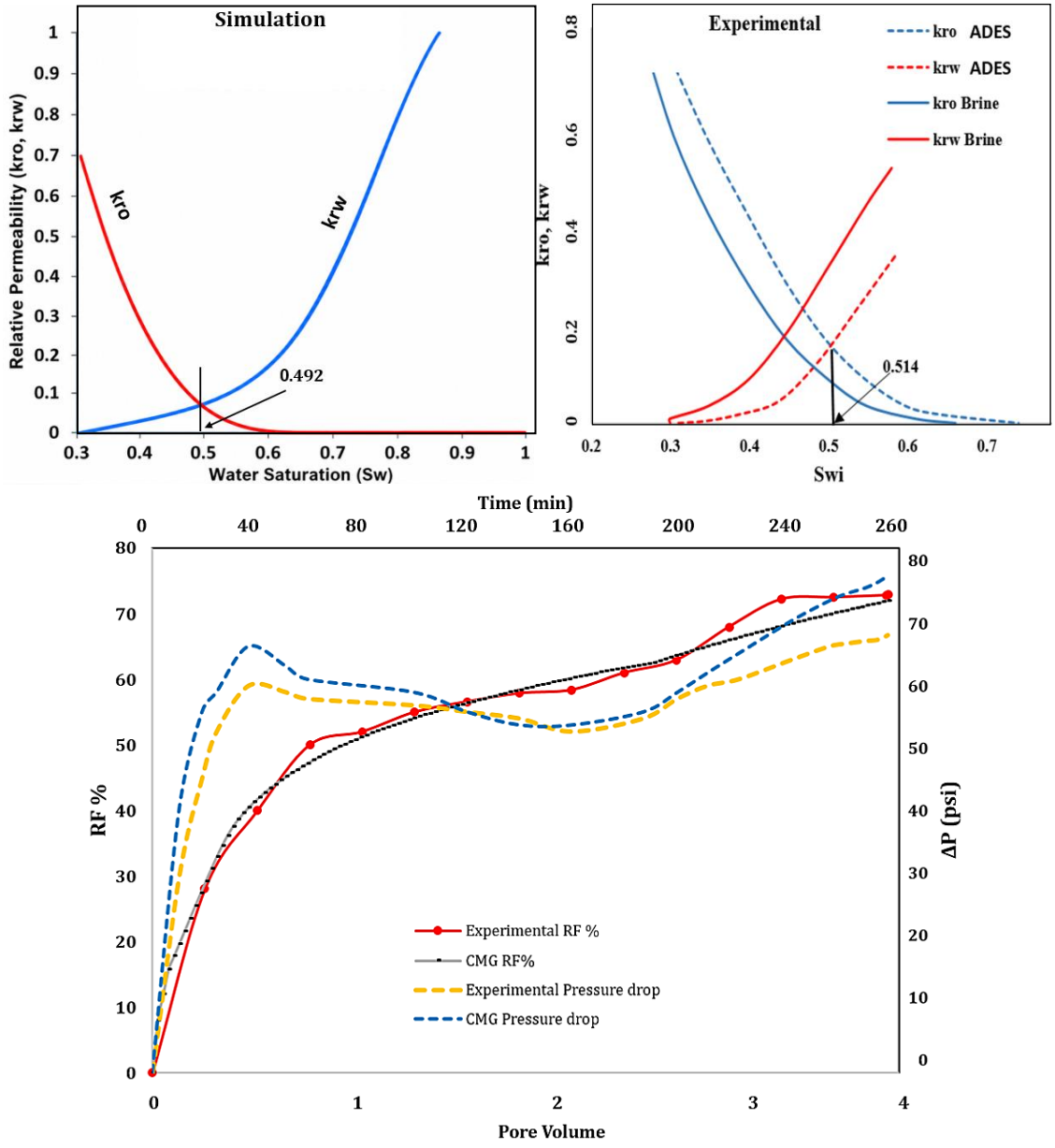

Figure 6. Oil Recovery Factor Profiles Obtained from Simulation and Experimental Result

The oil recovery factor is reproduced to within 5 % points and the pressure drop to within 6.5 % point, which is agreed with a 6 % points report by **(Kumar and Mandal, 2020)** for a zwitterionic surfactant injection . The match is closest between 1.5 and 2.5 PV, where the two pressure curves differ by less than 2 psi. Two regions are less well reproduced. The model over-predicts the early pressure maximum by about 10%, and it under-predicts recovery between 2.5 and 3.5 PV, reaching 63% against a measured 68% at 3 PV, indicating that the simulated tertiary response is delayed relative to the experiment. **(Tunnish et al., 2019)** report a comparable limitation, their match being satisfactory except for the pressure drop at the moment of slug injection.

The incremental recovery obtained here is of the same order as the 20 points reported by **(Kumar and Mandal, 2020)** for a zwitterionic surfactant in sandstone and considerably larger than the 4.6 points of **(Tunnish et al., 2019)**, consistent with the low oil viscosity of the present system relative to their 1200 cP heavy oil. It is, however, obtained with a 2 PV slug against the 0.3 PV of Kumar and Mandal, which motivates the slug-size optimization presented in their study. These comparisons should be interpreted cautiously because the studies differ in rock type, crude-oil viscosity, chemical formulation, and injected slug size.

Fig. 7 shows the cumulative oil production predicted by the CMG-STARS simulation of the ADES flooding process. Oil production increases over time, and at the end of the simulation period, approximately 4.5 cm^3 of oil is produced.

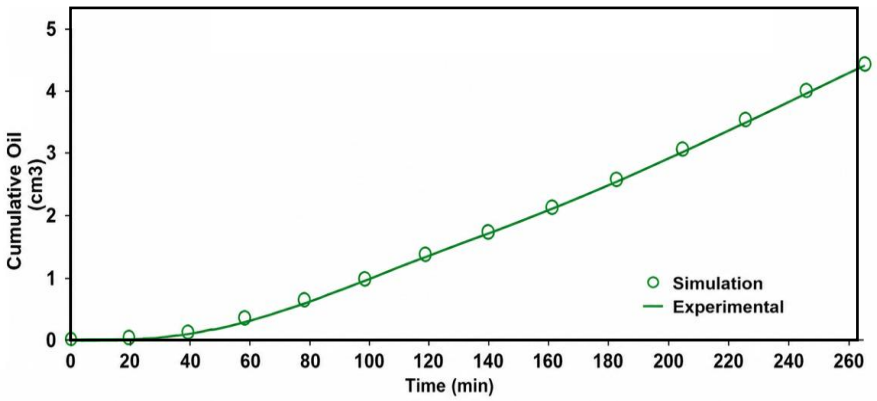

Figure 7. Accumulative Oil Production vs. Injection Time

In the early phase of the flooding, the net production rate rises gradually as the injected fluid is used to fill the pore volume and to form the displacement front. During flooding process, the production curve approaches a linear relationship, which is a stable displacement regime, and almost equal oil production rate. The good agreement between the reference experimental recovery data and the simulated results indicates that the history-matched numerical model adequately represents the core-flooding behavior observed in the laboratory, and the continued rise in cumulative oil production is in agreement with the decrease in oil saturation observed and is a result of the increase in micro-displacement efficiency of the ADES flooding.

Fig. 8 shows the spatial distribution of the ADES adsorption predicted with CMG-STARS in the carbonate core. The adsorption profile indicates that the maximum amount of adsorption is in the cells along the injection face, which is where the ADES first comes into contact with the rock surface. Intensity of adsorption decreases gradually from the inlet to the outlet, indicating the formation of an adsorption front in the porous media.

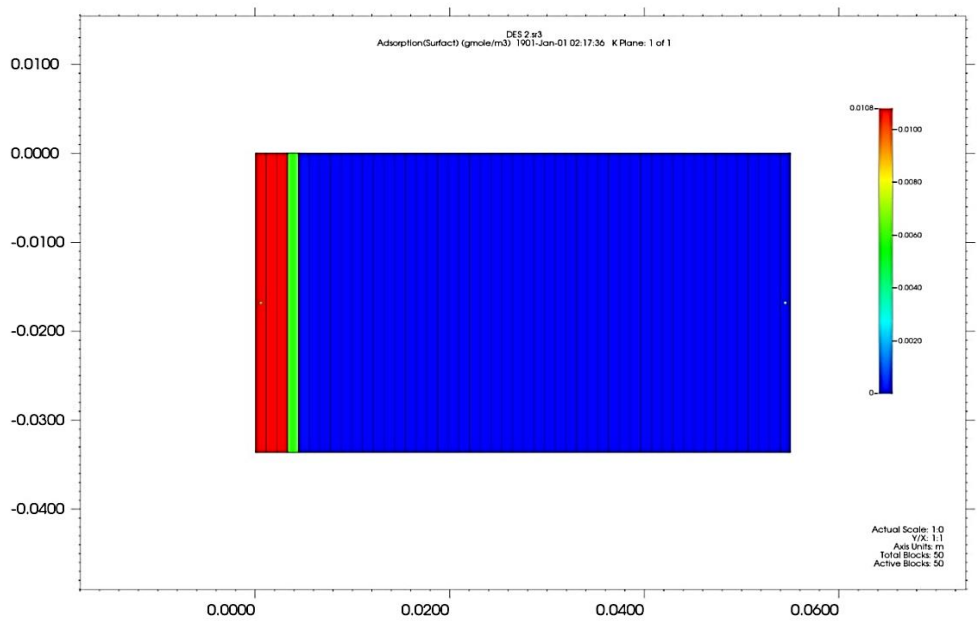

Figure 8. The ADES Adsorption Predicted with CMG-STARS

The simulated responses from the history matching showed an approximately linear adsorption behavior with the increase in ADES concentration, and this behavior provided the best agreement with the experimental core -flooding data. The highest adsorption takes place near the injection face where the concentration of ADES is the highest, and where there are many adsorption sites available. As the chemical front moves through the core the amount of adsorption is reduced toward the outlet due to progressive adsorption of the sites and the decrease in the concentration of the ADES in the flow path**.**

The spatial distribution of oil saturation predicted by the CMG-STARS simulation is shown in **Fig. 9** following the flooding with ADES. Color scale is used to show the range of decreasing oil saturation from about 0.69 (red) to about 0.42 (green) at the beginning of the injection. A low oil saturation zone was detected next to the injection side of the core, while the other part of the core has relatively high oil saturation. The progressive propagation of the displacement front through the porous medium is reflected by the progressive change from green to red. A reduction in the oil saturation at the injector is attributed to the effective microscopic displacement of oil due to the combined effect of wettability alteration, reduction in the oil/water interfacial tension and improvement in the mobility of the aqueous phase **(Pola et al., 2021; Raut et al., 2023)**. The nearly uniform displacement front yet again indicates flow stability with relatively little fingering or channeling, consistent with a one dimensional core of a homogeneous material

4.2 Sensitivity Analysis for the Parameters Affecting the Performance of ADES-EOR

A sensitivity analysis was carried out to assess the effect of the most important reservoir and operational parameters on the performance of the ADES flooding process. The main aim of this analysis was to find out the qualitative and quantitative effects of the various input parameters used on the objective functions of the simulation model. Knowing which parameters are the most influential will give useful information about the potential success or failure of the ADES flooding process.

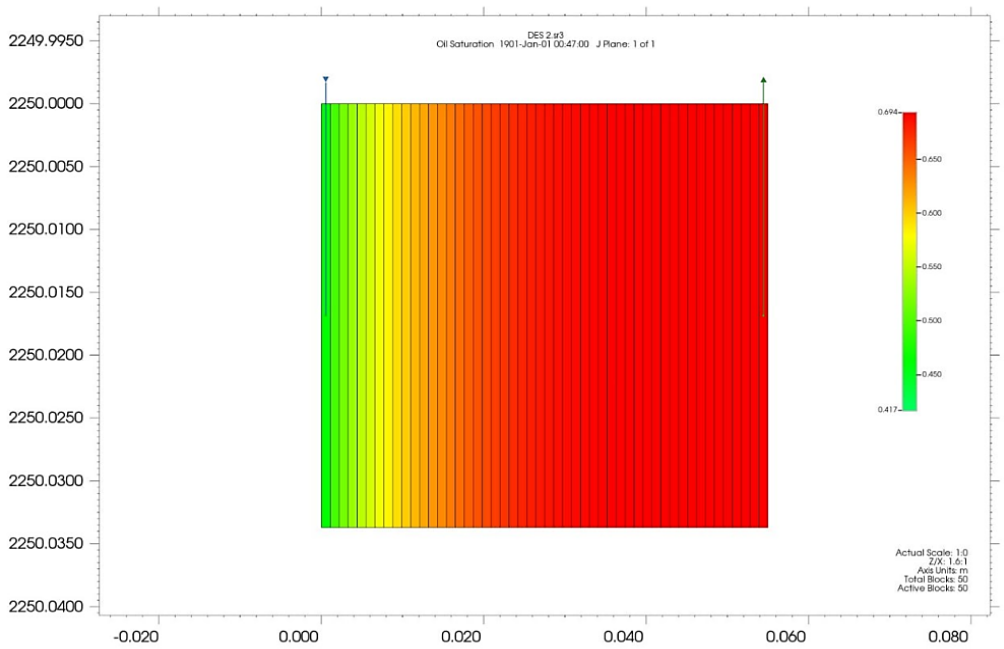

Figure 9. The Oil Saturation Predicted by CMG-STARS Simulation.

4.2.1 One Parameter at Time

Concentration of ADES, salinity, and effect of injection timing for ADES-EOR were investigated separately, while keeping all other parameters constant. As shown in **Fig. 10**, both oil recovery and cumulative oil production increased with increasing of ADES concentration. The increasing amount was about 4-5% for oil recovery factor and 0.5 cm^3 for cumulative oil at the simulation end.

The observed increase in oil recovery is consistent with the measured reduction in IFT and contact angle with increasing ADES concentration. The progressive accumulation of ADES molecules at the oil–water and rock–fluid interfaces can reduce interfacial free energy **(Jiang et al., 2024)** and promote a shift toward more water-wet conditions as shown in **Fig. 11** thereby improving microscopic oil displacement efficiency.

It can be concluded that the increase in ADES concentrations progressively reduces the oil–water IFT and contact angle. The IFT decreased from 4.22 mN/m at 0 ppm to 1.80 mN/m at 150 ppm and further decreased to 1.10 mN/m at the critical micelle concentration (CMC) of 200 ppm. Above the CMC, the reduction in IFT became less pronounced, decreasing only slightly from 1.10 mN/m at 200 ppm to 1.00 mN/m at 250 ppm. In contrast, the contact angle continued to decrease from 20.5° at the CMC to 8.4° at 250 ppm, indicating a continued shift toward strongly water-wet conditions. These changes in IFT and wettability can reduce capillary trapping and improve microscopic oil-displacement efficiency.

The reduction in contact angle can be attributed to the molecular interaction and adsorption of ADES molecules at the carbonate surface (Ahmadi et al., 2020). These interactions modify the solid–liquid interfacial properties and promote a shift of the carbonate surface toward more water-wet conditions. The continuous decrease in contact angle from 103° to 8.4° demonstrates a pronounced alteration of the carbonate wettability toward a strongly water-wet state.

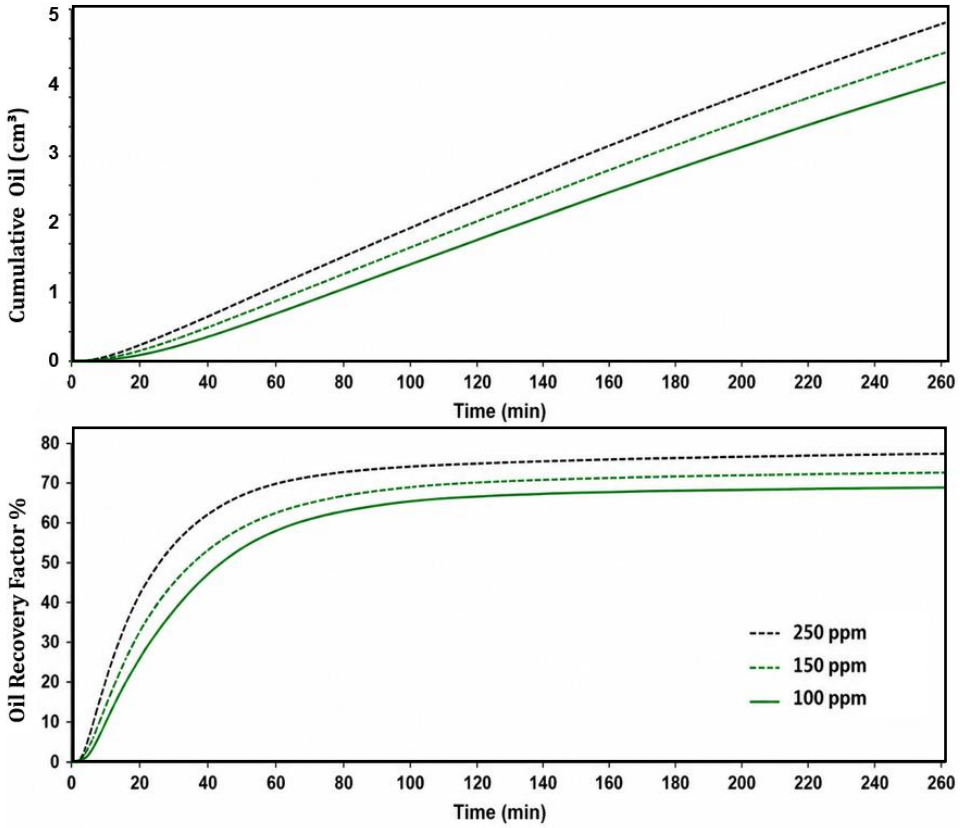

Figure 10. Effect of ADES Concentration on Oil Recovery Factor and Cumulative Oil Production Predicted by CMG-STARS Simulation

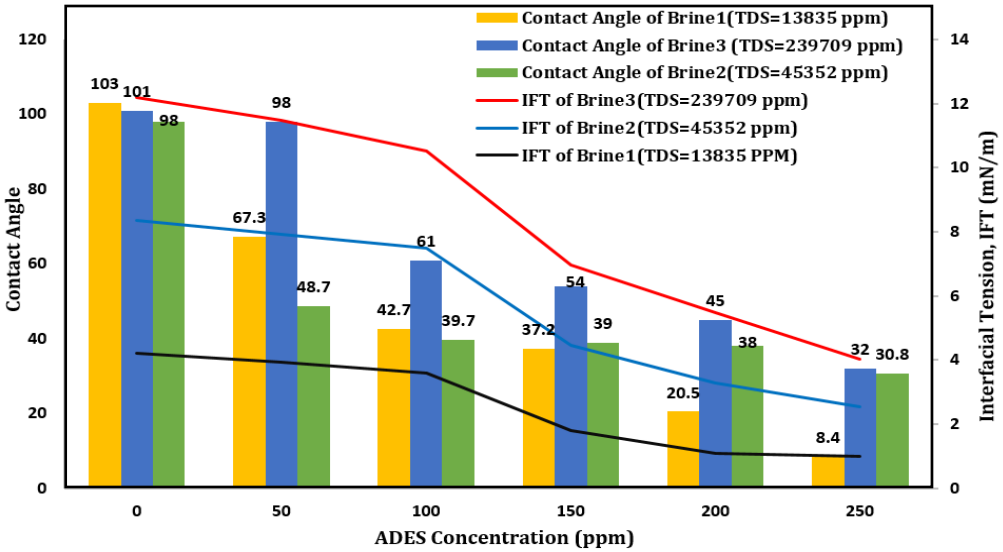

Figure 11. Effect of ADES Concentration on Contact Angle and Interfacial Tension at Different Brine Salinities.

The effect of brine salinity was also evaluated. As shown in **Fig. 12**, both the oil recovery factor and cumulative oil decrease with increasing brine salinity. This trend is similar to what was observed in the laboratory, where the effectiveness of the ADES system to lower the IFT and alter the wettability of the rocks decreased with increasing salinity as shown in **Fig. 11**, leading to lower oil recovery. Brine salinity had significant effects on the

performance of ADES. The lowest salt concentration brine1 (TDS = 13,835 ppm) showed the largest wettability change (most negative) and the lowest IFT over the range of ADES concentration tested in this study. For the brine 1, the contact angle decreased from 103° to 8.4° when ADES concentration was increased from 0 ppm to 250 ppm, whereas the contact angle for brine 2 decreased from 98° to 30.8° and that of brine 3 decreased from 101° to 32° when ADES concentrations increased from 0 ppm to 250 ppm. Likewise, the IFT was found to be consistently lower for Brine 1 than for the higher salinity brines. The results of this research show that the salinity of the brines decreased the effectiveness of ADES for the wettability alteration and IFT reduction, which could be due to changes in the ionic strength and specific ion–surface interactions of the carbonate system. Previous chemical EOR studies **(Belhaj et al., 2020)** show that the performance of the surfactant is dependent on salinity, which is in good agreement with the results presented herein. The salinity effect can be attributed to changes in ionic strength, salting-out behavior, and electrostatic screening. In particular, divalent ions (Mg^{2+}, Ca^{2+}) can compress the electrical double layer and reduce electrostatic repulsion between adsorbed molecules, thereby modifying interfacial packing and adsorption **(Ghaleh Golab, 2025; Haagh et al., 2017).**

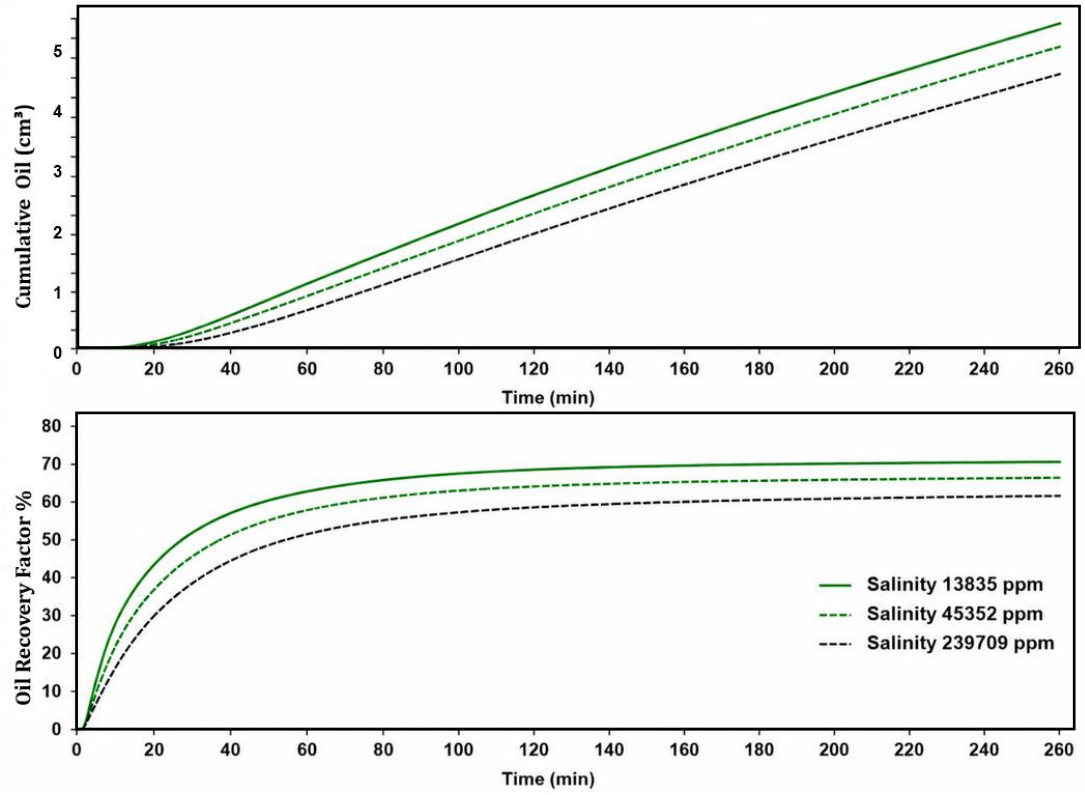

Figure 12. Effect of Brine Salinity on Oil Recovery Factor and Cumulative Oil Production Predicted by CMG-STARS Simulation

Finally, the effect of injection timing for ADES-EOR was investigated. The results showed that the delay in injecting ADES will have a negative impact on the flooding performance in terms of rate of oil production and recovery factor as shown in **Fig. 13**. **Fig.13(a)** is the result obtained when ADES is injected right after the brine flooding, without any delay between the two stages of injection. The ADES-injection case achieved a steadily increasing recovery factor compared to continuous brine injection, with an additional recovery of 7 % at 260 min. This enhancement suggests that early delivery of ADES would enable chemical to

interact with porous medium and residual oil with the presence of higher mobilizable oil content in the core. The opposite of this is illustrated in **Fig. 13(b)**, where the ADES is injected after the brine flooding. The profile between ADES-injection and brine-injection shows that the advantages of adding ADES to the brine are mostly eliminated if the injection is significantly delayed. These results show that the critical factor for the additional oil recovery with ADES injection is its timing. Early chemical injections help to achieve earlier wettability alteration and interfacial tension reduction, which in turn improves the displacement efficiency, leading to higher cumulative oil recovery. However, late surfactant injections will not recover the oil that has been trapped at the initial water flooding stage, which will be less overall.

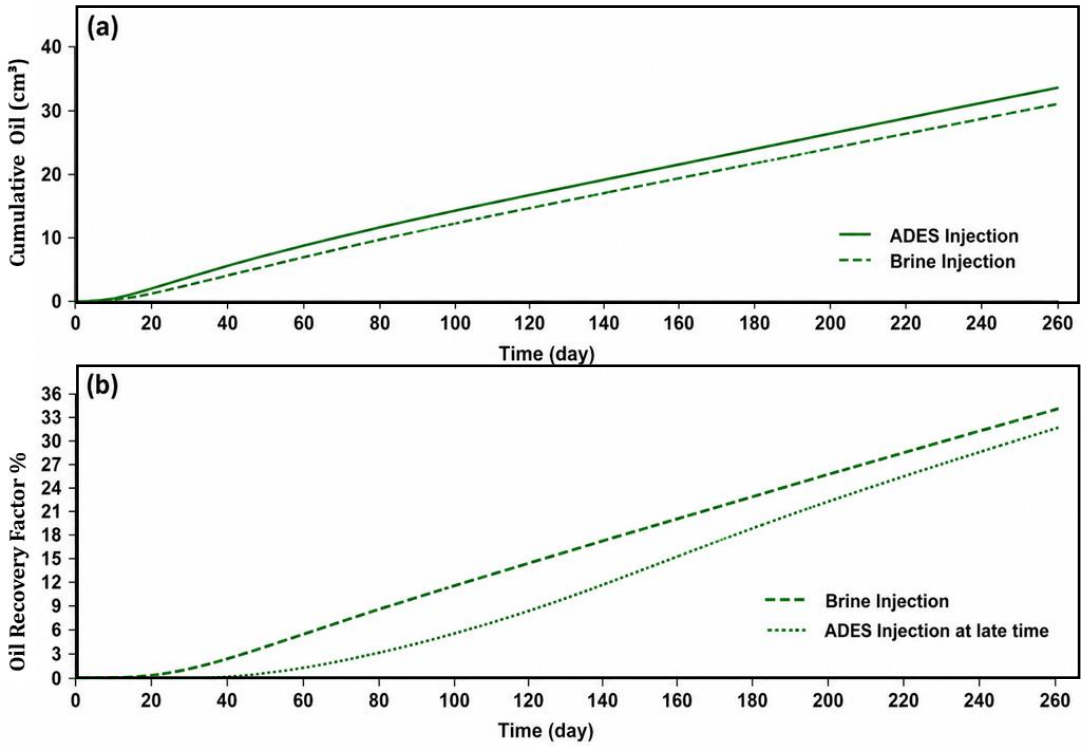

Figure 13. Effect of ADES Injection Timing on Core-Scale Oil Recovery Factor and Oil Production Rate Predicted by CMG-STARS Simulation

4.3 Contribution and Limitations

To the best of our knowledge this is the first time that amino-acid based deep eutectic solvents has begun to be tested as enhanced oil recovery agent for an Iraqi carbonate reservoir. The interfacial tension and contact angle between an alanine/choline chloride ADES and Mishrif crude on Mishrif carbonate were reported in the range of 0–250 ppm of ADES. The interfacial tension drops from 4.33 to 1 mN/m and the contact angle drops from 103° to 8.4° which means that the system switches from oil-wet to strongly water-wet in a concentration range spanning one to two orders of magnitude lower than the concentrations commonly used in surfactant flooding. These are measured parameters on a defined rock–fluid system and not transferred from analogue systems and are used to show that both mechanisms, the reduction of interfacial tension and the alteration of wettability, are active simultaneously for the same concentration interval in this solvent.

The following limitations restricted the conclusions of this study and define the work required for field application: the results are established at core scale, a linear core flood is not necessarily an aerial sweep, it does not account for gravity segregation and it does not account for the contrast in vertical permeability of the Mishrif interval. All measurements and simulations were performed at 25 °C. Interfacial tension, viscosity, adsorption capacity and the thermal stability of the eutectic mixture are all temperature dependent, and the interfacial and wetting measurements should be repeated at reservoir temperature. No cost analysis was performed.

5. CONCLUSIONS

1. The physicochemical characteristics of the prepared ADES were found to be suitable for the application in the enhanced oil recovery under the investigated conditions.
2. Increasing ADES concentration resulted in a substantial reduction in IFT and contact angle, indicating enhanced interfacial activity and a shift toward more water-wet carbonate conditions.
3. The measured IFT decreased from 4.22 to 1.00 mN/m, while the contact angle decreased from 103° to 8.4° as the ADES concentration increased from 0 to 250 ppm.
4. The ADES injection resulted in an incremental 15 percentage point increase in total recovery (73% of OOIP) and a 36 % decrease in residual oil saturation (0.290 to 0.186).
5. The controlling mechanism in this system is wettability alteration, rather than IFT: the contact angle decreased by 94.6°, altering the surface from oil-wet to strongly water-wet, whereas the interfacial tension fell by less than one order of magnitude, which is insufficient on its own to mobilize capillary-trapped oil.
6. Secondary brine flooding recovered 58% of OOIP in and reduced oil saturation from 0.690 to 0.290.
7. The history matches CMG-STARS model reproduced the measured recovery factor within 5 percent and the measured differential pressure within 6.5 percent. The match is closest between 1.5 and 2.5 PV, where the two pressure curves differ by less than 2 psi; the model over-predicts the early pressure maximum by about 10% and under-predicts recovery between 2.5 and 3.5 PV (63% simulated against 68% measured at 3 PV), indicating that the simulated tertiary response is delayed relative to the experiment.
8. The measured pressure response is not the result of the viscosity effect but is due to oil bank formation and to the change to the water-wet relative permeability set which results in lower water relative permeability at a given water saturation.
9. Brine composition controls the effectiveness of the solvent: over 0–250 ppm, the contact angle fell from 103° to 8.4° in brine 1 (13,835 ppm TDS), from 98° to 30.8° in brine 2 and from 101° to 32° in brine 3, and the interfacial tension was consistently lowest in brine 1.
10. The concentration selected for the core flooding simulation was 150 ppm, below the measured CMC of 200 ppm. Increasing the concentration above 150 ppm raised the recovery factor by only a further 4-5 percentage points across the whole 150-250 ppm range, while the mass of solvent retained by adsorption increased approximately linearly with concentration; 150 ppm therefore represents the most favorable ratio of incremental recovery to solvent consumed under the conditions tested, rather than the concentration of maximum recovery.
11. The conclusions are bounded by the conditions of the model: a homogeneous one-dimensional core at 25 °C and 14.7 psi pore pressure, without gravity segregation,

crossflow, areal sweep or reservoir heterogeneity, and with wettability alteration treated as instantaneous. Extension to field conditions requires a three-dimensional sector model and is not claimed here.

NOMENCLATURE

Symbol	Description	Symbol	Description
Ad_i	Adsorbed concentration of component *i*	P	Pressure, Pa
C	AADES concentration, kg/m^3 or mol/m^3	P_α	Pressure of phase (α), Pa
C_{ads}	Adsorbed AADES concentration on the rock surface	q_α	Source/sink term (injection or production rate)
$C_{i,\alpha}$	Mass fraction of component *i* in phase (α)	r_k	Reaction rate
D	Dispersion coefficient, m^2/s	$ratn$	Dimensionless interpolation parameter for the non-wetting phase
$D_{i,\alpha}$	Dispersion/diffusion coefficient of component *i* in phase (α), m^2/s	$ratw$	Dimensionless interpolation parameter for the wetting phase
$DTRAPNA$	Lower interpolation limit for the non-wetting phase	R_{ads}	Adsorption term
$DTRAPNB$	Upper interpolation limit for the non-wetting phase	S_α	Saturation of phase (α)
$DTRAPWA$	Lower interpolation limit for the wetting phase	S_o	Oil saturation
$DTRAPWB$	Upper interpolation limit for the wetting phase	S_{oirw}	Irreducible oil saturation
g	Gravitational acceleration, m/s^2	S_{orw}	Residual oil saturation
k	Absolute permeability, mD	S_w	Water saturation
k_r	Relative permeability	S_{wcon}	Connate water saturation
k_{ro}	Oil relative permeability	S_{wcrit}	Critical water saturation
k_{roA}	Oil relative permeability for set A	T_α	Phase transmissibility
k_{roB}	Oil relative permeability for set B	u_α	Darcy velocity of phase (α), m/s
k_{rocw}	Oil relative permeability at connate water saturation	V	Grid block volume, m^3
k_{rw}	Water relative permeability	V_f	Fluid volume
k_{rwA}	Water relative permeability for set A	V_r	Rock volume
k_{rwB}	Water relative permeability for set B	v_{ik}	Stoichiometric coefficient of component *i* in reaction *k*
kr_{wiro}	Water relative permeability at irreducible oil saturation	$WRCV$	Water relative permeability curve interpolation parameter
K_d	Adsorption coefficient	z	Elevation, m
Nc	Capillary number	$\Delta\varphi_\alpha$	Phase potential difference
Now	Corey exponent for oil relative permeability	∇	Gradient operator
Nw	Corey exponent for water relative permeability	$\emptyset$	Porosity
$OCRV$	Oil relative permeability curve interpolation parameter	ρ_α	Density of phase (α), kg/m^3
oil	Oil interpolation factor	μ_α	Viscosity of phase (α), Pa·s

Acknowledgements

This study was financially supported by the Petroleum Research and Development Center (PRDC), Ministry of Oil, Iraq, under Contract No.7/231/1328 (April 7, 2024), "Effect of Chemical Addtives on Wettablity Alteration during EOR". The authors are also grateful for the valuable technical support and cooperation provided by the College of Engineering, University of Baghdad and the Department of Chemical Engineering and Department of Petroleum Engineering.

Credit Authorship Contribution Statement

Elaf Q. Attieh: Conceptualization, Methodology, Investigation, Software, Formal analysis, Validation, Data curation, Visualization, Writing – original draft, Writing – review & editing. Hussein Q. Hussein: Supervision, Methodology, Validation, Writing – review & editing. Anfal K. Shebli: Resources, Project administration, Coordination with the Petroleum Research and Development Center.

Declaration of Competing Interest

The authors declare that they have no known competing financial interests or personal relationships that could have appeared to influence the work reported in this paper.

REFERENCES

Abdullah, R., Hussein, H., and Jali, R., 2026. Synergistic effect of different ions and hexadecyltrimethylammonium bromide on wettability alteration for carbonate rock. *Baghdad Science Journal*, 23(2), pp. 418–428. https://doi.org/10.21123/2411-7986.5193

Ahmadi, S., Hosseini, M., Tangestani, E., Mousavi, S.E., and Niazi, M., 2020. Wettability alteration and oil recovery by spontaneous imbibition of smart water and surfactants into carbonates. *Petroleum Science*, 17(3), pp. 712–721. https://doi.org/10.1007/s12182-019-00412-1

Akbar, M., Jenei, B., Lakos, M., Steffens, B., Kulaksiz, S., and Ganzer, L., 2026. Relative permeability uncertainty in geological CO_2 storage: A full-cycle scal-based modeling framework and its impact on long-term storage performance. *Research Square* (preprint).*

Alameedy, U., Fatah, A., Abbas, A., and Al-Yaseri, A., 2023. Matrix acidizing in carbonate rocks and the impact on geomechanical properties: A review. *Fuel*, 394, P. 128586. https://doi.org/10.1016/j.fuel.2023.128586

Al-Dujaili, A., Shabani, M., and AL-Jawad, M., 2023. Effect of heterogeneity on recovery factor for carbonate reservoirs: A case study for Mishrif Formation in West Qurna Oilfield, Southern Iraq. *Iraqi Journal of Chemical and Petroleum Engineering*, 24(3), pp. 103–111. https://doi.org/10.31699/IJCPE.2023.3.10

Al-Dujaili, A., Wei, Z., and Ghurab, A. S., 2026. Next-generation polymer flooding for enhanced oil recovery: A critical review of nano-reinforced formulations, hybrid injection strategies, and data-driven performance forecasting. *KJES*, 6, pp. 218–253. https://doi.org/10.63463/kjes1252.

Alquraishi, A., and Benzagouta, M., 2015. Efficiency of ionic liquids for chemical enhanced oil recovery. *Journal of Petroleum Exploration and Production Technology*, 5, pp. 353–361. https://doi.org/10.1007/s13202-014-0147-5

Atilhan, M., and Aparicio, S., 2021. Review on chemical enhanced oil recovery: Utilization of ionic liquids and deep eutectic solvents. *Journal of Petroleum Science and Engineering*, 205, P. 108746. https://doi.org/10.1016/j.petrol.2021.108746

Aziz, K., and Settari, A., 2002. *Petroleum Reservoir Simulation*. Applied Science Publishers, New York.

Belhaj, A., Elraies, K., Mahmood, S.M., Zulkifli, N., Akbari, S., and Hussien, O., 2020. The effect of surfactant concentration, salinity, temperature, and pH on surfactant adsorption for chemical enhanced oil recovery: A review. *Journal of Petroleum Exploration and Production Technology*, 10, pp. 125–137. https://doi.org/10.1007/s13202-019-0685-y.

Biyouki, A., Izadi, N., Bovard, S., Tahernezhad, Y., Nassar, N., and Ghafar-Zadeh, E., 2025. Comprehensive experimental study of multivariable oil–brine–rock interactions: Impact of brine–rock chemistry and crude oil polarity on enhanced oil recovery in carbonate reservoirs. *Scientific Reports*, 15, P. 25605. https://doi.org/10.1038/s41598-025-09448-3

Boon, J. A., 1984. Chemistry in enhanced oil recovery – an overview. *Journal of Canadian Petroleum Technology*, P. 23. https://doi.org/10.2118/84-01-08.

Buyukozer Ozkan, H., Terlemez, A., Batibay, A.B., Erdogan, H., and Kont Cobankara, F., 2024. Evaluation of surface tensions and root-dentin surface contact angles of different endodontic irrigation solutions. *BMC Oral Health*, 24, P. 681. https://doi.org/10.1186/s12903-024-04453-w.

Cazarez-Candia, O., Vital-Ocampo, A.G., and Montoya-Hernández, D., 2012. Volume-averaged mass equations for multiphase flow in porous media for in situ combustion. *Petroleum Science and Technology*, 30, pp. 201–211. https://doi.org/10.1080/10916461003792328.

Chen, Z., Huan, G., and Ma, Y., 2006. Computational methods for multiphase flows in porous media. *Society for Industrial and Applied Mathematics*. https://doi.org/10.1137/1.9780898718942.

Corey, A. T., 1977. *Mechanics of Heterogeneous Fluids in Porous Media*. Water Resources Publications, Fort Collins, Colorado, USA.

Delshad, M., Pope, G., and Sepehrnoori, K., 1996. A compositional simulator for modeling surfactant enhanced aquifer remediation: 1. Formulation. *Journal of Contaminant Hydrology*, 23, pp. 303–327. https://doi.org/10.1016/0169-7722(95)00106-9.

Elaghoury, M., Alarbah, A., Shirif, E., and Jia, N., 2022. Performance evaluation of ionic liquids using numerical simulation. *Advances in Chemical Engineering and Science*, 12, pp. 145–162. https://doi.org/10.4236/aces.2022.123011.

Ghaleh Golab, E., 2025. Evaluation of zwitterionic and polymeric surfactant adsorption for enhanced oil recovery in sandstone reservoirs with high salinity conditions. *Journal of Petroleum Exploration and Production Technology*, 15, P. 171. https://doi.org/10.1007/s13202-025-02089-2.

Goudarzi, A., Delshad, M., and Sepehrnoori, K., 2016. A chemical EOR benchmark study of different reservoir simulators. *Computers & Geosciences*, 94, pp. 96–109. https://doi.org/10.1016/j.cageo.2016.06.013.

Haagh, M.E.J., Siretanu, I., Duits, M.H.G., and Mugele, F., 2017. Salinity-dependent contact angle alteration in oil/brine/silicate systems: The critical role of divalent cations. *Langmuir*, 33, pp. 3349–3357. https://doi.org/10.1021/acs.langmuir.6b04470.

Hamdi, Z., Kumaran, P.N., and Talabi, O., 2020. Investigation and optimization of deep eutectic solvent in enhanced oil recovery using numerical simulation. *In: Abu Dhabi International Petroleum Exhibition & Conference*. https://doi.org/10.2118/202633-MS.

Hasan, M., 2022. Various techniques for enhanced oil recovery: A review. *International Journal of Oil, Gas and Coal Research,* 2, pp. 83–97. https://doi.org/10.55699/ijogr.2022.0201.1018.

Husain, A., and Abu-Jdayil, B., 2025. Natural deep eutectic solvent for exclusive and assured green enhanced oil recovery and other oil and gas applications: A review. *Journal of Molecular Liquids*, 434, P. 128019. https://doi.org/10.1016/j.molliq.2025.128019.

Imankulov, T., Lebedev, D., Matkerim, B., Daribayev, B., and Kassymbek, N., 2021. Numerical simulation of multiphase multicomponent flow in porous media: Efficiency analysis of Newton-based method. *Fluids*, 6, P. 355. https://doi.org/10.3390/fluids6100355.

Jalil, R., and Hussein, H., 2018. The influence of nanofluid compared with polyethylene glycol and surfactant on wettability alteration of carbonate rock. *In: IOP Conference Series: Materials Science and Engineering*, 454, article 012046. https://doi.org/10.1088/1757-899X/454/1/012046.

Jiang, W., Hou, Z., Yao, S., Wu, X., Gai, J., Nie, C., Su, X., Lu, S., Wang, Y., Huang, B., Dong, C., Liu, D., Jiang, J., Yu, X., Wang, Y., Zhang, J., Zhao, C., Yang, E., He, X., Qi, G., Li, J., Ma, Y., and Zhang, L., 2024. Research on the timing for subsequent water flooding in alkali-surfactant-polymer flooding in Daqing Oilfield based on automated machine learning. *Scientific Reports*, 14, P. 27897. https://doi.org/10.1038/s41598-024-79491-z.

Kumar, A., and Mandal, A., 2020. Core-scale modelling and numerical simulation of zwitterionic surfactant flooding: Designing of chemical slug for enhanced oil recovery. *Journal of Petroleum Science and Engineering*, 192, P. 107333. https://doi.org/10.1016/j.petrol.2020.107333.

Kumar, A., Medha, S., Chakraborty, D., Kundu, D., and Khan, S., 2025. Enhanced oil recovery promoted by aqueous deep eutectic solvents on silica and calcite surfaces: A molecular dynamics study. *Physical Chemistry Chemical Physics*, 27, pp. 9573–9589. https://doi.org/10.1039/D4CP04888A.

Kumar, S., and Mandal, A., 2017. Thermodynamics of micellization, interfacial behavior and wettability alteration of aqueous solution of nonionic surfactants. *Tenside Surfactants Detergents*, 54, pp. 427–436. https://doi.org/10.3139/113.110514.

Lake, L., Johns, R., Rossen, W., and Pope, G. A., 2014. Fundamentals of enhanced oil recovery. *Society of Petroleum Engineers*. https://doi.org/10.2118/9781613993286.

Little, J.E., and Kennedy, H.T., 1968. A correlation of the viscosity of hydrocarbon systems with pressure, temperature and composition. *Society of Petroleum Engineers Journal*, 8, pp. 157–162. https://doi.org/10.2118/1589-PA.

Liu, H., Chen, Z., Guo, X., and Shen, L., 2021. Development of a scalable thermal reservoir simulator on distributed-memory parallel computers. *Fluids*, 6, P. 395. https://doi.org/10.3390/fluids6110395.

Lwisa, E. G., 2021. Chemical enhanced oil recovery. *International Journal of Innovative Education and Research*, 9, pp. 160–172. https://doi.org/10.31686/ijier.vol9.iss6.3160.

Pola, J., Geiger, S., Mackay, E., Maier, C., and Al-Rudaini, A., 2021. Numerical simulations of surfactant flooding in carbonate reservoirs: The impact of geological heterogeneities across scales. *In: SPE Europec featured at 82nd EAGE Conference and Exhibition. SPE, Amsterdam, The Netherlands*. Paper D041S010R004. https://doi.org/10.2118/205180-MS.

Raut, D. S., Joshi, V. A., Khan, S., and Kundu, D., 2023. A-priori screening of deep eutectic solvent for enhanced oil recovery application using COSMO-RS framework. *Journal of Molecular Liquids*, 377, article 121482. https://doi.org/10.1016/j.molliq.2023.121482.

Salih, T. A., Sahi, S. H., and Al-Dujaili, A. N. G., 2016. Using different surfactants to increase oil recovery of Rumaila Field (experimental work). *IJCPE*, 17, pp. 11–31. https://doi.org/10.31699/IJCPE.2016.3.2.

Tunnish, A., Shirif, E., and Henni, A., 2019. History matching of experimental and CMG-STARS results. *Journal of Petroleum Exploration and Production Technology*, 9, pp. 341–351. https://doi.org/10.1007/s13202-018-0455-2.

Velez, C., and Acevedo, O., 2022. Simulation of deep eutectic solvents: Progress to promises. *WIREs Computational Molecular Science*, 12, P. e1598. https://doi.org/10.1002/wcms.1598.

Zhao, J., Wang, Q., Rong, W., Zeng, J., Ren, Y., and Chen, H., 2024. Permeability prediction of carbonate reservoir based on nuclear magnetic resonance (NMR) logging and machine learning. *Energies*, 17, article 1458. https://doi.org/10.3390/en17061458.

نمذجةٌ على مقياس اللبّ ومحاكاةٌ عدديّةٌ لحقن مذيبٍ يوتكتيكيٍّ عميقٍ قائمٍ على الألانين لتعزيز استخلاص النفط: دراسةُ حالةٍ مختبريّةٍ وحاسوبيّةٍ لمكمن المشرّف في حقل غرب القرنة–2 جنوبيَّ العراق

ايلاف قاسم عطيه * [1, 2]، حسين قاسم حسين [2]، انفال كريم شبلي [3]

[1] قسم الهندسة الكيمياوية، كلية الهندسة، جامعة بغداد، بغداد، العراق.

[2] معهد التدريب النفطي، ميسان، وزارة النفط، ميسان، العراق.

[3] مركز البحث والتطوير النفطي، وزارة النفط، بغداد، العراق.

الخلاصة

تبحث هذه الدراسة في تقييم أداء مذيب يوتكتيكي عميق قائم على الأحماض الأمينية (ADES)، يتكون من الألانين وكلوريد الكولين، بوصفه مذيبًا أخضر للإزاحة النفطية في مكمن المشرف الكربوناتي، وذلك بالاعتماد على نموذج عددي تمت معايرته مختبريًا. تمثلت أهداف الدراسة في قياس التوتر البيني (IFT) وتقييم تغير قابلية البلل لنظام المذيب اليوتكتيكي العميق القائم على الأحماض الأمينية/النفط الخام/الصخر الكربوناتي، بالإضافة إلى محاكاة تجربة إغراق اللب الصخري باستخدام برنامج CMG–STARS. أظهرت النتائج انخفاض التوتر البيني من 4.22 ملي نيوتن/متر وانخفاض زاوية التلامس من 103° إلى 1.00 ملي نيوتن/متر و8.4°، على التوالي، عند زيادة تركيز المذيب اليوتكتيكي العميق القائم على الألانين من 0 إلى 250 جزء بالمليون. وقد تم تطوير نموذج كارتيزي أحادي الأبعاد (50 × 1 × 1) باستخدام برنامج CMG–STARS، مع المحافظة على الحجم الكلي، وحجم المسام، ومساحة المقطع العرضي، وطول اللب الأسطواني. وتم تمثيل تغير قابلية البلل من خلال الاستيفاء الخطي بين النفاذية النسبية للحالة المحبة للنفط والحالة المحبة للماء، في حين تم تمثيل الاحتجاز الكيميائي باستخدام نموذج متساوي حرارة الامتزاز في CMG. أدى الإغراق بالمحلول الملحي إلى استخلاص 58% من النفط الأصلي في المكان (OOIP) ، مع انخفاض تشبع النفط من 0.690 إلى 0.290. وبعد ذلك، أدى الحقن الثالثي للمذيب اليوتكتيكي العميق القائم على الأحماض الأمينية بتركيز 150 جزء بالمليون إلى رفع معامل الاستخلاص إلى 73%، محققًا زيادة إضافية قدرها 15 نقطة مئوية من النفط الأصلي، إلى جانب انخفاض بنسبة 36% في تشبع النفط المتبقي، ليصل إلى 0.186. تمكن النموذج الذي تمت مطابقته تاريخيًا من إعادة إنتاج معامل الاستخلاص المقاس بفارق لا يتجاوز 5 نقاط مئوية، كما تمكن من تمثيل فرق الضغط بفارق لا يتجاوز 6.5 نقاط مئوية. وتتمثل المساهمة الرئيسية لهذه الدراسة في دمج القياسات التجريبية للتوتر البيني وزاوية التلامس ضمن عملية استيفاء النفاذية النسبية لتمثيل إغراق المذيب اليوتكتيكي العميق القائم على الأحماض الأمينية في نظام كربوناتي عراقي، وإثبات أن تغيير قابلية البلل، وليس خفض التوتر البيني، هو العامل المسيطر في التحكم بالاستخلاص النفطي الإضافي في هذا النظام.

الكلمات المفتاحية: المذيب العميق المشتق من الأحماض الأمينية، المكامن الكربوناتية، برنامجCMG–STARS ، تجارب الحقن خلال اللب الصخري، الاستخلاص المعزز للنفط.